"Gheorghe Asachi" Technical University of Iasi, Romania

PHOTOCATALYTIC ACTIVITY OF Ag/TiO₂–P25 MODIFIED CEMENT: OPTIMIZATION USING TAGUCHI APPROACH

Mohammad A. Behnajady[1]*, Sara Bimeghdar[1], Hamed Eskandarloo[2]

[1]Department of Chemistry, Tabriz Branch, Islamic Azad University, Tabriz, Iran
[2]College of Agriculture & Life Sciences, Cornell University, Ithaca, NY, USA

Abstract

In this study, Ag/TiO₂–P25 nanoparticles prepared via photodeposition method and its textural properties were characterized using X–ray diffraction (XRD), transmission electron microscopy (TEM), UV–vis diffuse reflectance spectroscopy (DRS), and N₂ physisorption techniques. The cements modified with TiO₂–P25 and Ag/TiO₂–P25 nanoparticles were immobilized on tile plates, and their photocatalytic activity was evaluated versus the removal of Erioglaucine as the model organic pollutant. The Ag/TiO₂–P25 modified cement showed the highest photocatalytic activity compared to TiO₂–P25 modified cement due to the positive effect of silver in trapping photogenerated electrons at conduction band of TiO₂. Also, the effect of operational variables such as initial Erioglaucine concentration, irradiation time, and UV–light intensity on the photocatalytic activity of Ag/TiO₂–P25 modified cement was investigated and optimized using the Taguchi approach. The optimum operational conditions were found to be: initial Erioglaucine concentration of 5 mg L^{-1}, irradiation time of 90 min and UV–light intensity of 55.9 W m^{-2}.

Key words: Ag/TiO₂–P25, fixed–bed system, modified cement, photocatalytic removal, Taguchi approach

1. Introduction

In recent years, advanced oxidation processes (AOPs) have been considered a very promising method to deal with the problem of organic pollutants removal in aqueous systems (Dulman et al., 2017; Eskandarloo et al., 2016). Among the AOPs, heterogeneous photocatalysis has been found as an emerging destructive technology leading to the total mineralization of variety of organic compounds with a low cost (Behnajady et al., 2011a). Heterogeneous photocatalysis involves a combination of UV light and a semiconductor catalyst (e.g. TiO₂ and ZnO), most often in suspension mode in aqueous solution (Behnajady et al., 2018; Chakrabarti et al., 2004). Titanium dioxide has attracted considerable attention as a suitable photocatalyst with strong oxidizing effect for the

widespread environmental applications (Behnajady et al., 2011b; Lutic et al., 2017; Zhou et al., 2005). When a photon is illuminated onto the TiO₂ catalyst with energy equal to or greater than band–gap energy, the electrons at valence band (e_{CB}^-) can be promoted to the conduction band, leaving the positive holes (h_{VB}^+) behind (Fujishima et al., 1972) according to Eq. (1):

$$TiO_2 + hv \rightarrow e_{CB}^- + h_{VB}^+ \qquad (1)$$

The positive hole can oxidize water and hydroxyl ions to produce the highly reactive hydroxyl radical (Xiong et al., 2013), according to Eqs. (2) and (3):

$$H_2O + h_{VB}^+ \rightarrow {}^{\bullet}OH + H^+ \qquad (2)$$

$$^-OH + h_{VB}^+ \rightarrow {}^{\bullet}OH \qquad (3)$$
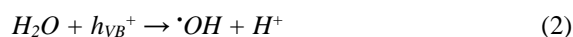
*Author to whom all correspondence should be addressed: e-mail: behnajady@gmail.com, behnajady@iaut.ac.ir; Phone: +98–411–3396136; Fax: +98–411–3333458

The hydroxyl radicals are powerful oxidants which can be used to oxidize most organic contaminants (Mohammadzadeh et al., 2016; Sizykh et al., 2018), according to Eq. (4) and Eq. (5):

$$S + {}^{\bullet}OH \rightarrow Int. \tag{4}$$

$$Int. + {}^{\bullet}OH \rightarrow P \tag{5}$$

where: *S*, *Int.* and *P* are Erioglaucine, intermediates and final mineralization molecules, respectively.

The photocatalytic activity of TiO_2 nanoparticles can be affected by many factors such as the particle size; anatase and rutile phase content, band gap, surface area and pore volume (Behnajady and Eskandarloo, 2013a). The photocatalytic efficiency of TiO_2 nanoparticles is limited to the recombination rate of photogenerated electron–hole pairs. In order to reduce electron–hole recombination, various methods have been used, including rare earth metal and transition metal ions doping and coupling other semiconductors (Parida et al., 2008).

During recent years, modification of cementitious materials as catalyst supporting media has attracted considerable attention due to their porous structure and strong binding ability that are suitable for immobilizing catalysts (Chen and Poon, 2009). Metal oxide powders can be easily mixed with cement-bonded construction materials without additional treatments. The preparation of the photocatalyst–modified cements can be beneficial for the development of self–cleaning building material surfaces (Lackhoff et al., 2003).

Lackhoff et al. (2003) prepared TiO_2 and ZnO modified cement and reported higher photocatalytic activity for TiO_2 modified cement. Khataee et al., (2011) modified cement with different TiO_2 nanomaterials (TiO_2 in the form of Degussa P25, Millennium PC500, Millennium PC105 and anatase-Merck) and reported higher photocatalytic activity for TiO_2 in the form of Degussa P25. To our best knowledge, the photocatalytic activity of Ag/TiO_2–P25 modified cement has not yet been reported. Based on our previous studies, silver-doped TiO_2 nanoparticles have shown considerable photocatalytic activity in the removal of various organic pollutants from aqueous solution (Behnajady et al., 2008; Behnajady and Eskandarloo, 2013a; Behnajady and Eskandarloo, 2013b); therefore, we are interested in using Ag/TiO_2–P25 nanoparticles for cement modification.

In this study, first, Ag/TiO_2–P25 nanoparticles were prepared via photodeposition of silver onto TiO_2–P25, and then the prepared nanoparticles were used for modification of white cement. Photocatalyst modified cements were immobilized on tile plates and their photocatalytic activity was evaluated versus the removal of Erioglaucine as the model organic pollutant. The textural properties of TiO_2–P25 and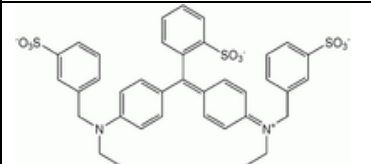 Ag/TiO_2–P25 nanoparticles were characterized using XRD, TEM, DRS, and BET techniques and their effect on photocatalytic properties of modified cement was compared with each other. Also, the effect of operational variables such as initial Erioglaucine concentration, irradiation time, and UV–light intensity on the photocatalytic activity Ag/TiO_2–P25 modified cement was investigated. The Taguchi approach was applied to identify the optimal conditions and to select the parameters having the most important effect on the photocatalytic removal rate.

2. Experimental

2.1. Materials

Titanium dioxide nanoparticles (TiO_2–P25) containing 80% anatase and 20% rutile with a surface area of about 56.81 m^2 g^{-1} and primary particle size of 24 nm were purchased from the Degussa Co. in Germany. Erioglaucine, as the model organic pollutant purchased from ACROS Organics. Silver nitrate was purchased from Merck Co., also located in Germany. The chemical structure and other characteristics of Erioglaucine are listed in Table 1.

Table 1. Chemical structure and characteristics of Erioglaucine

Molecular formula	$C_{37}H_{34}N_2Na_2O_9S_3$
λ_{max}	625 nm
Molar mass	792.86 g/mol
Colour index no.	42090
Other names	Acid Blue 9, Alzen Food Blue No. 1, Atracid Blue FG, Eriosky blue, Patent Blue AR, Xylene Blue VSG, C.I. 42090
Structure	

2.2. Preparation of Ag/TiO_2–P25 nanoparticles

The Ag/TiO_2–P25 nanoparticles were prepared by photoreducing of Ag^+ ions to Ag metal onto the TiO_2 in the following stages: First, 3 g of TiO_2–P25 was added to 100 mL deionized water. The pH of the TiO_2–P25 suspension was adjusted to 3; then the required amount of $AgNO_3$ (0.5 mol%) was added to the TiO_2–P25 suspension. The mixtures were then irradiated with UV–C light (30 W, λ_{max} = 254 nm, mercury lamp, Philips, Holland) for 3 h and then dried in an air oven at 100°C for 24 h. The dried solids were calcined at 400°C for 3 h.

2.3. Modification of cement with Ag/TiO_2–P25 nanoparticles and immobilization on tile plate

To prepare the Cement – Ag/TiO_2–P25 sample, cement and Ag/TiO_2–P25 nanoparticles were

mixed in the ratio of 2 : 1 (2 g cement : 1 g nanoparticles for each plate). Then, the suitable amount of deionized water was added to the mixture in order to obtain a uniform suspension. The obtained suspension was immobilized physically on the surface of the tile plate (5 cm × 5 cm). The prepared sample was placed at room temperature for 24 h and was left to dry. After drying, the tile plate was washed with deionized water for the removal of weakly attached samples.

2.4. Characterization methods

XRD patterns (used for phase identification) and crystallite size calculations were recorded with a Siemens D5000 X–ray diffraction using Cu Kα radiation. The (1 0 1) peak ($2\theta = 25.28°$) of anatase and the (1 1 0) peak ($2\theta = 27.42°$) of rutile were used for analysis. The average crystallite size of the particles was calculated through the line broadening of corresponding XRD peaks using the Scherrer's equation (Patterson, 1939):

$$D = \frac{k\lambda}{\beta \cos\theta} \tag{6}$$

where: D is the average crystallite size (nm), λ is the wavelength of the X–ray radiation, k is a constant equal to 0.89, β is the full width at half maximum intensity and θ is the half diffraction angle.

The phase content in the samples can be calculated by Eq. (7) (Spurr and Myers, 1957):

$$Rutile\ phase\% = \frac{100}{1 + 0.8\left(\dfrac{I_A}{I_R}\right)} \tag{7}$$

where: I_A is the integrated intensity of anatase (101) diffraction peak and I_R is the integrated intensity of rutile (110) diffraction peak.

The size of the TiO₂–P25 and Ag/TiO₂–P25 nanoparticles was measured with TEM instrument (Philips CM–10 HT–100 keV). Nitrogen adsorption–desorption was carried out using Belsorp mini II instrument to measure the specific surface area, mean pore diameter and total pore volume of TiO₂–P25 and Ag/TiO₂–P25 nanoparticles using the Brunauer–Emmett–Teller (BET) and the Barret–Joyner–Halender (BJH) methods.

UV–vis DRS of samples was obtained using AvaSpec–2048 TEC spectrometer to determine the optical band gap (E_g) of TiO₂–P25 and Ag/TiO₂–P25 nanoparticles. To determine the E_g, the Eq. (8) was used:

$$\alpha(h\nu) = B(h\nu - E_g)^{1/2} \tag{8}$$

where: α is optical absorption coefficient, B is a constant dependent on the transition probability, h is the Plank's constant and ν is the frequency of the

radiation. The E_g values were calculated by plotting $(\alpha h\nu)^2$ versus $h\nu$, followed by extrapolation of the linear part of the spectra to the energy axis (Al Abdul–Kader, 2009).

2.5. Photocatalytic activity measurement

Photocatalytic removal operations were carried out at room temperature in a batch photoreactor of 150 mL in volume. UV–light irradiation was provided with a 30 W (UV–C) mercury lamp (Philips, Holland) emitting around 254 nm. Light source was placed above the photoreactor. In each run, a tile plate loaded with Ag/TiO₂–P25 modified cement was inserted in the photoreactor. Then, the desired concentration of Erioglaucine (10 mg L⁻¹) was transferred into the photoreactor and stirred for 30 min in the dark with magnetic stirrer. The photocatalytic reaction was initiated by turning on the light source. At given irradiation time intervals, the samples (5 mL) were taken out, and then the Erioglaucine concentration was analyzed by UV–vis spectrophotometry (Pharmacia Biotech, Ultrospec 2000, England). Blank experiments under UV light irradiation alone (photolysis) and also adsorption process after 30 min indicate 14 and 5.5 removal percent, respectively.

2.6. Experimental design

The Taguchi method applies to fractional factorial experimental designs, called orthogonal arrays, to reduce the number of experiments while obtaining statistically meaningful and worthwhile results. The main stage in the design of an experiment is the selection of control parameters; therefore, as many parameters as possible need to be considered, and non–meaningful variables must be identified at the earliest opportunity. The Taguchi method creates an orthogonal array to meet these requirements. The selection of a suitable orthogonal array depends on the number of control parameters and their levels (Engin et al., 2008; Mousavi et al., 2007). Three selected control parameters and their levels employed in this work are listed in Table 2. These control parameters include irradiation time, initial Erioglaucine concentration, and light intensity.

Table 2. Experimental variables and their levels

Variable	Symbol	Levels		
		1	2	3
Initial Erioglaucine concentration (mg L⁻¹)	A	5	10	15
Irradiation time (min)	B	30	60	90
Light intensity (W m⁻²)	C	23.9	39.5	55.9

All control parameters have three levels. The L9 orthogonal array was selected by the Taguchi method. The number of experiments required is drastically reduced to nine. This means that nine experiments with different combinations of the parameters should be conducted in order to study the

main effects and interactions. In the classical combination method, using full factorial experimentation would require $3^3 = 27$ experiments to capture the effective parameters.

3. Results and discussion

3.1. Characterization of TiO_2–P25 and Ag/TiO_2–P25 nanoparticles

Fig. 1 shows the XRD patterns of TiO_2–P25 and Ag/TiO_2–P25 (1 mol%) nanoparticles. Results show a combination of anatase and rutile phases for both samples. Absence of characteristic peaks corresponding to the Ag can be due to low Ag dopants content and also appropriate dispersion of Ag onto TiO_2–P25 surface (Li et al., 2007). XRD patterns reveal that the crystalline phases in TiO_2–P25 and Ag/TiO_2–P25 nanoparticles exist as a mixed anatase/rutile phases. Eq. (6) was employed to calculate the average crystallite size of samples, using reflections of anatase at 25.3°. The average crystallite size is estimated to be 22 nm for TiO_2–P25 and Ag/TiO_2–P25 samples.

The particle size of the Ag/TiO_2–P25 nanoparticles was investigated by TEM analysis. The TEM image in Fig. 2 show that the samples have irregular shape and agglomerated to larger particles. The size of the Ag/TiO_2–P25 nanoparticles obtained from TEM image was about 20 nm, which corresponded to the crystallite size calculated by using the XRD patterns.

Nitrogen adsorption and desorption isotherms of the TiO_2–P25 and Ag/TiO_2–P25 nanoparticles (Fig. 3) showed type–III isotherm of the IUPAC

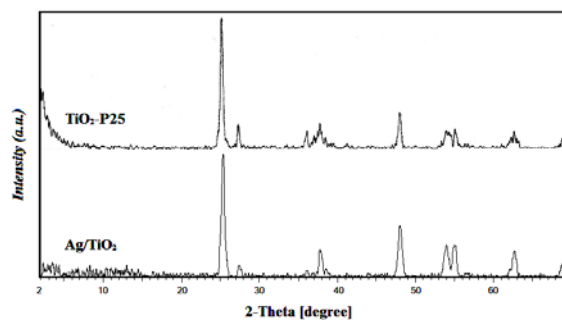classifications, which indicates a mesoporous structure (Alvar et al., 2010).

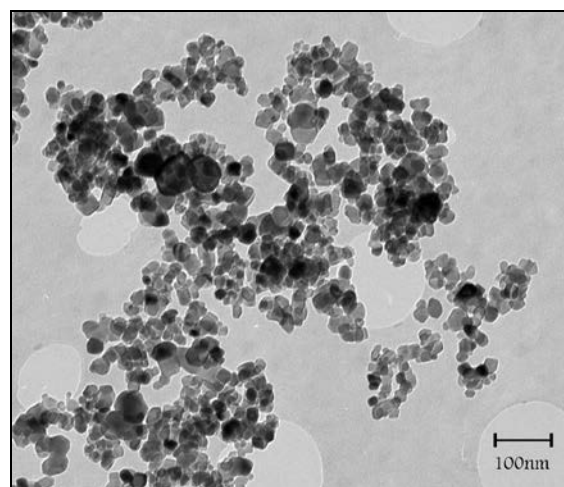**Fig. 1.** XRD patterns of TiO_2–P25 and Ag/TiO_2–P25 nanoparticles

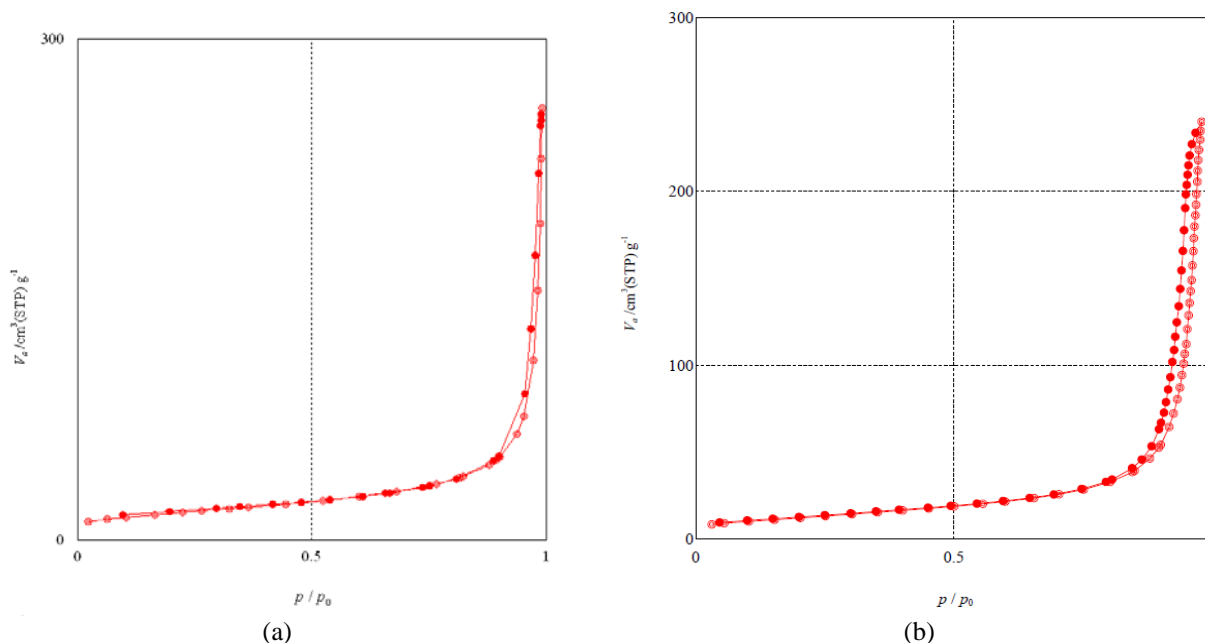**Fig. 2.** TEM image of the Ag/TiO_2–P25 nanoparticles

(a)   (b)

Fig. 3. Nitrogen adsorption–desorption isotherms of TiO_2–P25 (a) and Ag/TiO_2–P25 (b) nanoparticles
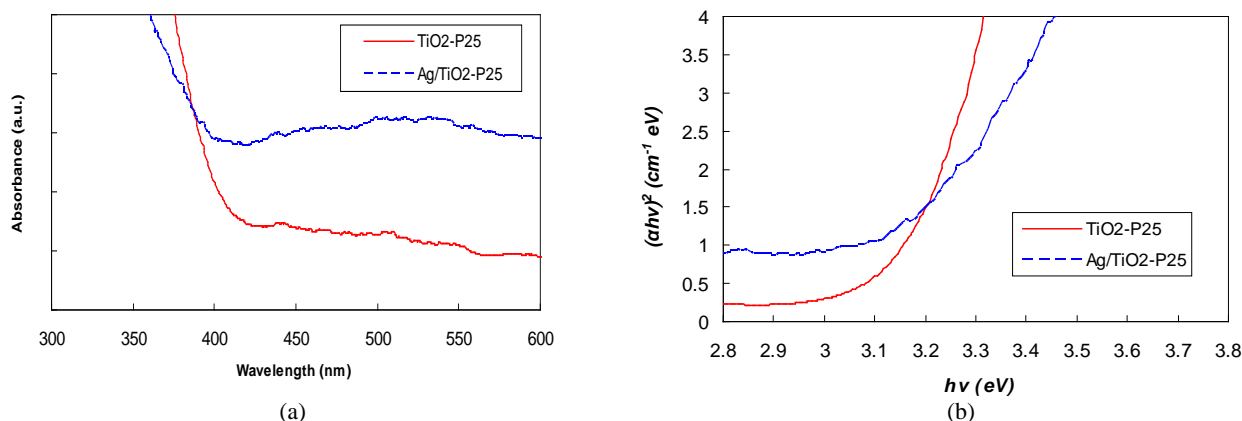
(a)

(b)

Fig. 4. The diffuse reflectance spectroscopy spectra (a) and plot of $(\alpha h v)^2$ versus $h v$ (b) for
TiO_2–P25 and Ag/TiO_2–P25 nanoparticles

The BET surface area and total pore volume for Ag/TiO_2–P25 nanoparticles, as determined by N_2 physisorption experiments, were 44.28 m² g⁻¹ and 0.371 cm³ g⁻¹, respectively, whereas the BET surface area and total pore volume for pure TiO_2–P25 nanoparticles were 56.81 m² g⁻¹ and 0.387 cm³ g⁻¹, respectively. The value of BET surface area for Ag/TiO_2–P25 nanoparticles was less than bare TiO_2–P25 nanoparticles, indicating that photodeposition of Ag had a strong impact on reducing surface area of TiO_2–P25. To study the effect of Ag photodeposition on the optical absorption properties of TiO_2–P25 nanoparticles, DRS was carried out. Fig. 4a shows the optical absorption of TiO_2–P25 and Ag/TiO_2–P25 nanoparticles. The absorption wavelength for Ag photodeposited TiO_2–P25 nanoparticles is significantly red shifted. The doped samples show a long tail extending up to 410 and 440 nm for TiO_2–P25 and Ag/TiO_2–P25 nanoparticles, respectively. The tail absorption can be due to the formation of impurity levels within the band gap of TiO_2 which shifts the band edge absorption to visible light region (Wang et al., 2011). The values of E_g were calculated by extrapolation of the linear part of the spectra to the energy axis (Fig. 4b). The E_g values for TiO_2–P25 and Ag/TiO_2–P25 nanoparticles were estimated to be 3.17 and 3.10 eV. The results indicate that Ag photodeposition into TiO_2–P25 decreased optical band gap energy.

3.2. Photocatalytic activity

A comparison of pure TiO_2–P25 and Ag photodeposited TiO_2–P25 nanoparticles for photocatalytic removal of the Erioglaucine pollutant was made in the slurry form. Fig. 5 shows the removal of a 10 mg L⁻¹ Erioglaucine solution in the presence of TiO_2–P25 and Ag photodeposited TiO_2–P25 nanoparticles. It can be observed that the highest removal efficiency was obtained by using Ag/TiO_2–P25 nanoparticles. The positive effect of Ag on the photocatalytic activity of TiO_2–P25 nanoparticles could be accounted for by its ability to modify the interfacial charge transfer to electron acceptors such

as oxygen and trapping electrons. When Ag comes into contact with TiO_2–P25, due to the formation of Schottky barrier in Ag and TiO_2 contact region and because the Fermi level of Ag is lower than that of TiO_2 conduction band, electrons produced at conduction band of TiO_2–P25 will transfer to Ag (Behnajady and Eskandarloo, 2013b; Seery et al., 2007). On the other hand, free holes at valence band of TiO_2–P25 react with adsorbed water molecules and hydroxide ions to produce hydroxyl radicals as reactive species in the photodegradation process (El-Kemary et al., 2011; Ren et al., 2009). Finally, photodeposition of Ag onto TiO_2–P25 provides the separation of electron–hole pairs, resulting in the improvement of TiO_2–P25 photocatalytic activity.
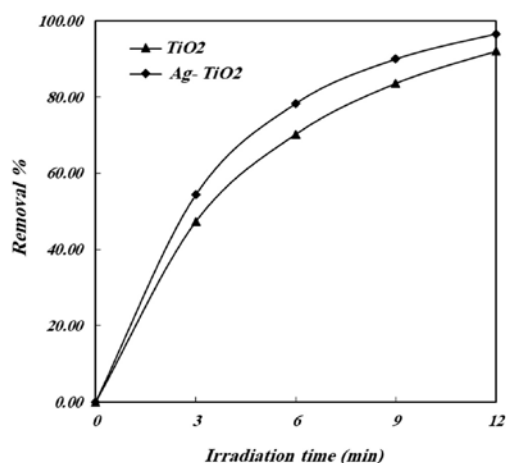

Fig. 5. Photocatalytic removal of Erioglaucine in the presence of TiO_2–P25 and Ag/TiO_2–P25 nanoparticles ([AB9]₀ = 10 mg L⁻¹, LI = 55.9 W m⁻², [catalyst] = 400 mg L⁻¹ and pH neutral)

Fig. 6 shows a comparison of Erioglaucine (10 mg L⁻¹) removal in the presence of pure cement, TiO_2–P25 modified cement, and Ag/TiO_2–P25-modified cement immobilized on tile plates under UV–light irradiation. The results clearly indicate that Ag/TiO_2–P25-modified cement has the highest photocatalytic activity than other samples. This can be a consequence of the positive effect of Ag

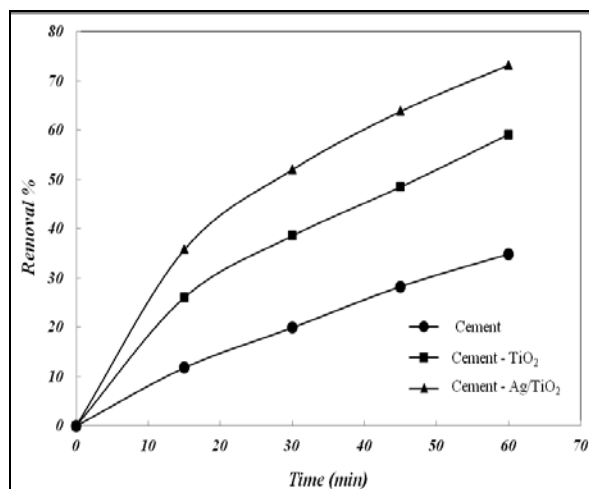photodeposition on the photocatalytic activity of TiO₂–P25 nanoparticles, as explained in the previous section.

Fig. 6. Photocatalytic removal of Erioglaucine in the presence of pure cement and cement modified with TiO₂–P25 and Ag/TiO₂–P25 nanoparticles immobilized on tile plates ([AB9]$_0$ = 10 mg L^{-1}, LI = 55.9 W m^{-2}, and pH neutral)

3.3. Optimization of operational variables effect using Taguchi approach

The effect of operational variables such as initial Erioglaucine concentration, irradiation time, and UV–light intensity was investigated and optimized using the Taguchi approach. The structure of Taguchi's L9 design and the results of Erioglaucine removal percent in the presence of immobilized Ag/TiO₂–P25 modified cement are shown in Table 3. Average response and 'Quality Characteristics: Bigger is Better' were used to optimize the process. In this study, the average response analysis is based upon the removal percent of Erioglaucine, and its values are reported in Table 3. The analysis was performed by averaging the removal percent data of each experiment and plotting the values in a graphical form. Figs. 7a - 7c show the average response graph for Erioglaucine removal in the presence of Ag/TiO₂–P25 modified cement under different operational conditions. The peak points in these plots show the optimum conditions. In order to find out the effect of Erioglaucine concentration on photocatalytic removal efficiency of Ag/TiO₂–P25 modified cement, the experiments were carried out with initial Erioglaucine concentration ranging from 5 to 15 mg L^{-1} (Fig. 7a). From an application standpoint, it is important to study the dependence of photocatalytic removal efficiency on the initial concentration of pollutant. As seen in Fig. 7a, an increase in the initial concentration of Erioglaucine from 5 to 15 mg L^{-1} decreases the removal rate of Erioglaucine. This could be due to the fact that with increasing Erioglaucine concentration, the solution becomes impermeable to UV–light radiation, and thus the UV photons get intercepted before they can

reach the Ag/TiO₂–P25 modified cement surface (Rauf et al., 2009; Gupta et al., 2012). On the other hand, with more and more increase of Erioglaucine concentration, organic substances and intermediates are adsorbed on the surface of Ag/TiO₂–P25 modified cement, causing the generation of active species such as hydroxyl radicals reduce (Bu et al., 2011). Photocatalysis reaction efficiency largely depends on the absorption of light by photocatalyst. As seen in Fig. 7b, the removal rate of Erioglaucine increased by increasing irradiation time from 30 to 90 min in the presence of Ag/TiO₂–P25 modified cement. In order to find out the effect of UV–light intensity on photocatalytic removal rate of Erioglaucine, the experiments were carried out with light intensity ranging from 23.9 to 55.9 W m^{-2} (Fig. 7c). As the Figure shows, removal efficiency of Ag/TiO₂–P25 modified cement increased through increasing the UV–light intensity. The UV–light irradiation generates the photons needed for the electron transfer from the valence band to the conduction band of a photocatalyst. Therefore, when the UV–light intensity is low, electron–hole separation competes with recombination and decreases the formation of hydroxyl radicals (Neppolian et al., 2002; Petrovič et al., 2012). The removal rate of Erioglaucine increases when more radiations fall on the Ag/TiO₂–P25 modified cement surface and hence more hydroxyl radicals are produced. According to the obtained results shown in Figs. 7a - 7c, maximum Erioglaucine removal percentage in the presence of immobilized Ag/TiO₂–P25 modified cement can be obtained by setting the level 1 for 'initial Erioglaucine concentration' (5 mg L^{-1}), level 3 for 'irradiation time' (90 min), and level 3 for 'UV–light intensity' (62 W m^{-2}).

Table 3. Experimental layout using the L9 orthogonal array and experimental results for Erioglaucine removal in the presence of immobilized Ag/TiO₂–P25 modified cement

Run	Initial Erioglaucine concentration (mg L^{-1})	Irradiation time (min)	Light intensity (W m^{-2})	Removal (%)
1	1	1	1	42.47
2	1	2	2	69.5
3	1	3	3	8.97
4	2	1	2	37.55
5	2	2	3	70.36
6	2	3	1	56.15
7	3	1	3	42.19
8	3	2	1	47.05
9	3	3	2	67.58

The Analysis of variance (ANOVA) was employed as the statistical procedure to test the significance and adequacy of the model. The results of ANOVA (Table 4) shows that irradiation time had the largest variance. UV–light intensity and initial Erioglaucine concentration were in the second and third places, respectively.
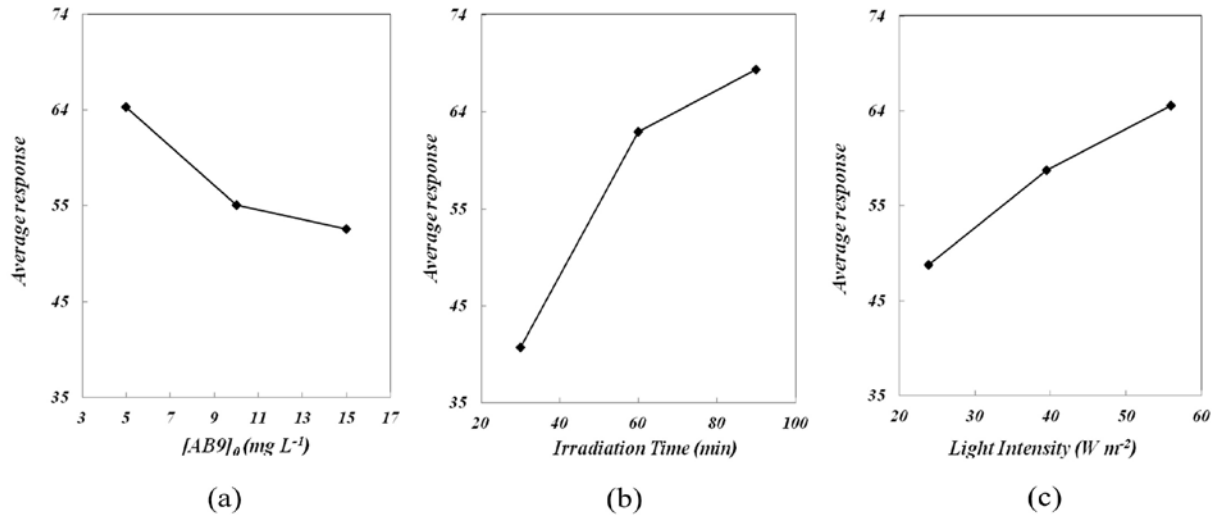
Fig. 7. Average response for effect of initial Erioglaucine concentration (a), irradiation time (b) and light intensity (c) on Erioglaucine removal in the presence of immobilized Ag/TiO$_2$–P25 modified cement

Table 4. Results of Analysis of Variance (ANOVA)

Source	Sum of squares	Degree of freedom	Variance	F–Ratio	Pure Sum	Percent
A	258.12	2	129.06	6.61	219.11	11.07
B	1278.86	2	639.43	32.78	1239.84	62.67
C	402.29	2	201.15	10.31	363.28	18.36
Error	39.02	2	19.51	–	–	7.9

Fig. 8 demonstrates the relative impact of each operational variable on the photocatalytic efficiency of Ag/TiO$_2$–P25 modified cement in removal of Erioglaucine. Consequently, it can be concluded that the irradiation time is the most effective parameter.
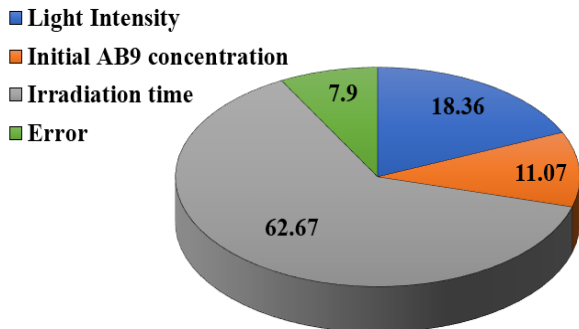

Fig. 8. Relative importance (%) of the operational variables on the photocatalytic efficiency of Ag/TiO$_2$–P25 modified cement in removal of Erioglaucine

4. Conclusions

White cement was modified with Ag photodeposited TiO$_2$–P25 nanoparticles and then immobilized on tile plates. Photocatalytic properties of Ag/TiO$_2$–P25 modified cement was evaluated in the removal of Erioglaucine under UV light irradiation and showed the high photocatalytic activity compared to TiO$_2$–P25 modified cement due to positive effect of silver in trapping of photogenerated electrons at conduction band of TiO$_2$.

Textural properties of TiO$_2$–P25 and Ag/TiO$_2$–P25 nanoparticles were characterized using different techniques. The effect of operational variables on the photocatalytic efficiency of Ag/TiO$_2$–P25 modified cement was optimized using the Taguchi approach.

References

Al Abdul-Kader A.M., (2009), Modification of the optical band gap of polyethylene by irradiation with electrons and gamma rays, *Philosophical Magazine Letters*, **89**, 162-169.

Alvar E.N., Rezaei M., Alvar H.N., (2010), Synthesis of mesoporous nanocrystalline MgAl$_2$O$_4$ spinel via surfactant assisted precipitation route, *Powder Technology*, **198**, 275-278.

Behnajady M.A., Dadkhah H., Eskandarloo H., (2018), Horizontally rotating disc recirculated photoreactor with TiO$_2$-P25 nanoparticles immobilized onto a HDPE plate for photocatalytic removal of p-nitrophenol, *Environmental Technology*, **39**, 1061-1070.

Behnajady M.A., Eskandarloo H., (2013a), Characterization and photocatalytic activity of Ag–Cu/TiO$_2$ nanoparticles prepared by sol–gel method, *Journal of Nanoscience and Nanotechnology*, **13**, 548-553.

Behnajady M.A., Eskandarloo H., (2013b), Silver and copper co–impregnated onto TiO$_2$–P25 nanoparticles and its photocatalytic activity, *Chemical Engineering Journal*, **228**, 1207-1213.

Behnajady M.A., Eskandarloo H., Modirshahla N., Shokri M., (2011a), Investigation of the effect of sol–gel synthesis variables on structural and photocatalytic properties of TiO₂ nanoparticles, *Desalination*, **278**, 10-17.

Behnajady M.A., Eskandarloo H., Modirshahla N., Shokri M., (2011b), Sol–gel low–temperature synthesis of stable anatase–type TiO₂ nanoparticles under different conditions and its photocatalytic activity, *Photochemistry and Photobiology*, **87**, 1002-1008.

Behnajady M.A., Modirshahla N., Shokri M., Rad B., (2008), Enhancement of photocatalytic activity of TiO₂ nanoparticles by silver doping: photodeposition versus liquid impregnation methods, *Global Nest Journal*, **10**, 1-7.

Bu X., Zhang G., Guo Y., (2011), Thermal modified palygorskite: Preparation, characterization, and application for cationic dye–containing wastewater purification, *Desalination and Water Treatment*, **30**, 39-347.

Chakrabarti S., Dutta B.K., (2004), Photocatalytic degradation of model textile dyes in wastewater using ZnO as a semiconductor catalyst, *Journal of Hazardous Materials*, **112**, 269-278.

Chen J., Poon C.S., (2009), Photocatalytic cementitious materials: influence of the microstructure of cement paste on photocatalytic pollution degradation, *Environmental Science & Technology*, **43**, 8948-8952.

Dulman V., Ignat M.E., Ignat L., Gânju D. Popa V.I., (2017), Decolorization of chlorolignin with hydrogen peroxide in the presence of silica [bis (dibenzoylmethido) copper II] as catalyst, *Environmental Engineering and Management Journal*, **16**, 2199-2210.

El-Kemary M., Abdel-Moneam Y., Madkour M., El-Mehasseb I., (2011), Enhanced photocatalytic degradation of Safranin–O by heterogeneous nanoparticles for environmental applications, *Journal of Luminescence*, **131**, 570-576.

Engin A.B., Özdemir Ö., Turan M., Turan A.Z., (2008) Color removal from textile dye bath effluents in a zeolite fixed bed reactor: Determination of optimum process conditions using Taguchi method, *Journal of Hazardous Materials*, **159**, 348-353.

Eskandarloo H., Badiei A., Behnajady M.A., Mohammadi Ziarani G., (2016), Hybrid Homogeneous and Heterogeneous Photocatalytic Processes for Removal of Triphenylmethane Dyes: Artificial Neural Network Modeling, *Clean–Soil, Air, Water*, **44**, 809-817.

Fujishima A., Honda K., (1972), Electrochemical photolysis of water at a semiconductor electrode, *Nature*, **238**, 37-38.

Gupta V.K., Jain R., Agarwal S., Nayak A., Shrivastava M., (2012), Photodegradation of hazardous dye quinoline yellow catalyzed by TiO₂, *Journal of Colloid and Interface Science*, **366**, 135-140.

Khataee A. R., Amani-Ghadim A.R., Rastegar Farajzade M., Valinazhad Ourang O., (2011), Photocatalytic activity of nanostructured TiO₂-modified white cement, *Journal of Experimental Nanoscience*, **6**, 138-148.

Lackhoff M., Prieto X., Nestle N., Dehn F., Niessner R., (2003), Photocatalytic activity of semiconductor–modified cement-influence of semiconductor type and cement ageing, *Applied Catalysis B: Environmental*, **43**, 205-216.

Li Y., Peng S., Jiang F., Lu G., Li S., (2007), Effect of doping TiO₂ with alkaline–earth metal ions on its photocatalytic activity, *Journal of the Serbian Chemical Society*, **72**, 393-402.

Lutic D., Coromelci C.G., Juzsakova T., Cretescu I., (2017), New mesoporous titanium oxide-based photoactive materials for the removal of dyes from wastewaters, *Environmental Engineering and Management Journal*, **16**, 801-807.

Mohammadzadeh M., Behnajady, M.A., Eskandarloo H., (2016), Hybridized advanced oxidation processes involving $UV/H_2O_2/S_2O_8^{2-}$ for photooxidative removal of p-nitrophenol in an annular continuous-flow photoreactor, *Kinetics and Catalysis*, **57**, 768-775.

Mousavi S.M., Yaghmaei S., Jafari A., Vossoughi M., Ghobadi Z., (2007), Optimization of ferrous biooxidation rate in a packed bed bioreactor using Taguchi approach, *Chemical Engineering and Processing*, **46**, 935-940.

Neppolian B., Choi H.C., Sakthivel S., Arabindoo B., Murugesan V., (2002), Solar/UV–induced photocatalytic degradation of three commercial textile dyes, *Journal of Hazardous Materials*, **89**, 303-317.

Parida K.M., Sahu N., (2008), Visible light induced photocatalytic activity of rare earth titania nanocomposites, *Journal of Molecular Catalysis A: Chemical*, **287**, 151-158.

Patterson A.L., (1939), The Scherrer formula for X–ray particle size determination, *Physical Review*, **56**, 978-982.

Petrovič V., Ducman V., Škapin S.D., (2012), Determination of the photocatalytic efficiency of TiO₂ coatings on ceramic tiles by monitoring the photodegradation of organic dyes, *Ceramics International*, **38**, 1611-1616.

Rauf M.A., Ashraf S.S., (2009), Fundamental principles and application of heterogeneous photocatalytic degradation of dyes in solution, *Chemical Engineering Journal*, **151**, 10-18.

Ren L., Zeng Y.P., Jiang D., (2009), Preparation, characterization and photocatalytic activities of Ag–deposited porous TiO₂ sheets, *Catalysis Communications*, **10**, 645-649.

Seery M.K., George R., Floris P., Pillai S.C., (2007), Silver doped titanium dioxide nanomaterials for enhanced visible light photocatalysis, *Journal of Photochemistry and Photobiology A: Chemistry*, **189**, 258-263.

Sizykh M.R., Batoeva A.A., Khandarkhayeva M.S., (2018), Removal of dyes from water by galvanocoagulation, *Environmental Engineering and Management Journal*, **17**, 27-34.

Spurr R.A., Myers H., (1957), Quantitative analysis of anatase–rutile mixtures with an X–ray diffractometer, *Analytical Chemistry*, **29**, 760-762.

Wang Q., Xu S., Shen F., (2011), Preparation and characterization of TiO₂ photocatalysts co–doped with iron (III) and lanthanum for the degradation of organic pollutants, *Applied Surface Science*, **257**, 7671-7677.

Xiong S., George S., Ji Z., Lin S., Yu H., Damoiseaux R., France B., Ng K.W., Loo S.C.J., (2013), Size of TiO₂ nanoparticles influences their phototoxicity: An in vitro investigation, *Archives of Toxicology*, **87**, 99-109.

Zhou M., Yu J., Cheng B., Yu H., (2005), Preparation and photocatalytic activity of Fe–doped mesoporous titanium dioxide nanocrystalline photocatalysts, *Materials Chemistry and Physics*, **93**, 159-163.